J. Fluid Mech. (2006), *vol.* 549, *pp.* 253–271.
doi:10.1017/S0022112005007615 Printed in the United Kingdom

The influence of buoyancy contrasts on miscible source–sink flows in a porous medium with thermal inertia

By MATS S. NIGAM AND ANDREW W. WOODS

BP Institute for Multiphase Flow, Madingley Rise, Madingley Road, Cambridge CB3 0EZ, UK

(Received 13 July 2004 and in revised form 5 July 2005)

We investigate the displacement of one fluid through an inclined porous sheet by the injection of a second fluid of different density. Using numerical simulation we explore the role of the density contrast between the injected and the reservoir fluid on the displacement process, in the cases where the density contrast originates from either compositional contrasts and/or temperature contrasts between the fluids. In the case where the density contrast originates from compositional differences between the fluids, the density front moves with the fluid–fluid front, and gravity may accelerate or decelerate the time for the injected liquid to reach the sink. In the case where the density contrast originates from a temperature contrast between the injected fluid and the reservoir fluid, then the density front follows the thermal front. Therefore, owing to thermal inertia, it lags behind the fluid–fluid front. This has a quantitative impact on the time required for the injected liquid to reach the sink. If there are both thermal and compositional contrasts between the injected and reservoir fluid, then the thermal and compositional fronts become decoupled in space. The two fronts may lead to complementary or opposing density changes; the different cases lead to vastly different patterns of displacement and time at which the injected liquid reaches the sink, even if the net change in density between reservoir and the injected fluid is the same. We discuss the implications of these phenomena for water injection in sub-surface hydrocarbon and geothermal reservoirs. In an Appendix, we note how a viscosity across both the thermal front and the fluid–fluid front can also lead to a rich spectrum of flow patterns, especially if one front is stable and the other unstable to viscous instability.

1. Introduction

During the recovery of hydrocarbons from sub-surface porous rock, operators often inject water to displace the hydrocarbons to the production wells and maintain the pressure in the reservoir. Typically, the liquid injected has a different temperature and composition from any geological water which is trapped with the hydrocarbons within the reservoir. Analogously, in geothermal systems, cold water is injected into the reservoir to displace the hot geothermal fluid to the production wells, and thereby mine the heat from the system (Elder 1997). As the injected water migrates through the rock, it will exchange heat with the rock, and owing to the thermal inertia, this will generate a thermal front which lags behind the fluid front (Fayers 1962; Phillips 1991). The compositional contrast between the injected and reservoir water may lead to a density contrast at the fluid–fluid interface. However, in addition, the thermal front

within the injected water may lead to a second density front (Phillips 1991; Menand, Raw & Woods 2002). In the recovery of heavy oil, steam is often injected with a view to heating up the rock and oil. This produces a decrease in oil viscosity across the thermal front, thereby enhancing the recovery, although the process depends on the effects of immiscible fractional flow (cf. Fayers 1962) since it is the residual oil which is of prime interest in that application.

The purpose of this paper is to explore the flow patterns which develop in a rectangular domain, with an internal source and sink, subject to these two evolving interfaces across which the density of the fluids may change. The work builds on other studies of miscible displacement in porous layers (Fayers 1962; Karakas, Saneie & Yortsos 1986; Chen & Meiburgh, 1998*a*, *b*, 1999), but is distinct in that there are two evolving interfaces across which there is a density contrast. In the Appendix, we include a discussion of the effects which a change in viscosity across the thermal front may have on the flow pattern, focusing on the interaction of this front and any change in viscosity across the fluid–fluid front. Many studies have focused on the interference of mobility contrasts across a displacement front (Gorell & Homsy 1983; Yortsos & Huang 1986; Loggia, Salin & Yortsos 1999), but the new feature of the present Appendix is the interaction of two fronts, which gradually spread apart, and across each of which there is a different jump in mobility.

Although the present work is strictly only relevant for miscible displacements, it does also provide important insight into the behaviour of immiscible displacements in the limit of relatively high permeability rock or rapid displacement, such that the interfacial tension between the fluids has a secondary impact on the flow. Indeed, with relatively rapid flow and a large interwell spacing, the capillary transition zone between the injected fluid and the original reservoir fluid remains relatively narrow (Lake 1996). In addition, with such immiscible displacements, the fractional flow of one phase increases rapidly with saturation up to a critical saturation beyond which the fractional flow increases more slowly to a maximum value when the saturation has reached its maximum. This leads to formation of the classic Buckley–Leverett shock front, across which there is a sharp jump in the saturation from purely reservoir fluid downstream to dominantly injected fluid upstream (Bear 1972). Although there may be a dispersive tail of reservoir fluid behind the shock front, in the case of a steep fractional flow curve, this will be small, and as a result, there is a well-defined interface between the fluids (Fayers 1962; Bear 1972; Karakas *et al.* 1986; Lake 1996). The new aspect of the present work is our investigation of the effect of the density contrasts on the sweep pattern.

In the case of a miscible displacement, there may be some dispersive mixing across the fluid–fluid front. The extent of this mixing region depends on the dispersion coefficient which is typically a function of the flow rate and the pore size and structure (Bear 1972; Phillips 1991). Typical values in permeable rocks vary over a wide range of values, 10^{-5}–$10^{-8}\,\mathrm{m^2\,s^{-1}}$. Over a time scale of, say, 10^7 s for fluid to migrate 100–1000 m, the mixed zone may grow to a distance of 1–10 m. For the lower end of this range, the mixed zone is very small compared to the fluid–fluid displacement scale.

Guided by these limits, in this work we model the motion of each of the fluid phases and the interfaces by making the simplifying assumption that the fluid properties vary continuously over the flow domain. We then model the motion of the fluid–fluid interface and the thermal front by tracking the motion of one field to represent the concentration of the injected fluid and a second field to denote the temperature. We assume that these fields evolve according to an advection–diffusion equation, with

the advection speed of the thermal field being a fraction of that of the fluid (Fayers 1962; Phillips 1991). This approach is analogous to the models of Chen & Meiburg (1998*a*, *b*, 1999) and strictly applies for miscible displacements, but has a more general application if the mixing zone between the fluids is narrow and so the dynamics are largely controlled by the density ratio, rather than the mixing zone.

In the following sections, we first introduce the model and the numerical technique. We then analyse the impact of a density contrast, which is advected with the flow, on the pattern of sweep in a source–sink geometry. We explore the balance between the strength of the buoyancy-induced pressure difference and the applied pressure difference between the source and sink on the flow pattern. We then illustrate the more complex density profile and flow patterns which may develop if the injected fluid is of both different temperature and different composition so that there are two density fronts within the flow domain. We examine the impact of the two density fronts on a source–sink flow within the same flow geometry; we focus on the evolving flow pattern and illustrate how the thermal and compositional fronts influence the fraction of the flow domain which is invaded with injected fluid prior to injected liquid reaching the sink. In an Appendix, we briefly discuss the effect that changes in the viscosity across the thermal front may have, and illustrate the pattern of the flow when there are viscosity contrasts across both the thermal and fluid–fluid fronts.

2. Formulation

As outlined in § 1, we adopt Darcy's law to describe the motion of fluid through a porous medium,

$$\boldsymbol{u}^* = -\frac{\boldsymbol{K}^*}{\phi\mu^*(C,\,T^*)}\cdot(\nabla^* p^* - [\rho^*(C,\,T^*) - \rho^*_{res}]\boldsymbol{g}^*\sin\theta), \tag{2.1}$$

$$\nabla^*\cdot\boldsymbol{u}^* = 0, \tag{2.2}$$

$$\frac{\partial C}{\partial t^*} + \nabla^*\cdot(\boldsymbol{u}^* C) = \nabla^*\cdot\left(D^*\frac{\boldsymbol{u}^*\boldsymbol{u}^*}{|\boldsymbol{u}^*|}\cdot\nabla^* C\right), \tag{2.3}$$

$$\frac{\partial T^*}{\partial t^*} + \nabla^*\cdot(\lambda\boldsymbol{u}^* T^*) = \nabla^*\cdot\left(\lambda D^*\frac{\boldsymbol{u}^*\boldsymbol{u}^*}{|\boldsymbol{u}^*|}\cdot\nabla^* T^*\right). \tag{2.4}$$

Asterisks are used to denote dimensional quantities. $\boldsymbol{u}^*$ and p^* are the Darcy or transport velocity and pressure, respectively. $\boldsymbol{K}^*$ is the permeability and ϕ the porosity of the rock, while $\mu^*(C,\,T^*)$ denotes the dynamic viscosity which for the majority of runs will be taken as constant, $\mu^*(C,\,T^*)=\mu^*$. The influence of viscosity contrasts is explored in the Appendix. ρ^* denotes densities and the subscript *res* stands for reservoir, while $\boldsymbol{g}^*\sin\theta$ is the component of the acceleration due to gravity parallel to the plane of the reservoir. C is the concentration of the injected fluid and T^* is its temperature. λ is the ratio of the advection speed of the thermal front, across which the density of the injected fluid is assumed to change, compared to the fluid–fluid front, and D^* is the dispersion coefficient for the mixing across the fronts. The porous matrix is taken as a constant, isotropic medium, $\boldsymbol{K}^* = k^*\boldsymbol{I}$, where k^*, ϕ and D^* are constants and $\boldsymbol{I}$ is the identity matrix. For convenience, we introduce the following scalings

$$\boldsymbol{u}^* = U^*\boldsymbol{u}, \quad \boldsymbol{x}^* = L^*\boldsymbol{x}, \quad t^* = (L^*/U^*)t, \quad T^* = T^*_{res} + \Delta T^*\,T,$$
$$D^* = L^* D, \quad p^* = (\phi\mu^* U^* L^*/k^*)\,p,$$

where L^* is the largest extent of the reservoir, and U^* is the velocity of the fluid at the injection well. With these scalings, equations (2.1)–(2.4) reduce to,

$$\boldsymbol{u} = -\nabla p + C(B_1 + T(B_2 - B_1))\hat{\boldsymbol{g}}, \tag{2.5}$$

$$\nabla \cdot \boldsymbol{u} = 0, \tag{2.6}$$

$$\frac{\partial C}{\partial t} + \nabla \cdot (\boldsymbol{u}C) = \nabla \cdot \left(D \frac{\boldsymbol{u}\boldsymbol{u}}{|\boldsymbol{u}|} \cdot \nabla C \right), \tag{2.7}$$

$$\frac{\partial T}{\partial t} + \nabla \cdot (\lambda \boldsymbol{u}T) = \nabla \cdot \left(\lambda D \frac{\boldsymbol{u}\boldsymbol{u}}{|\boldsymbol{u}|} \cdot \nabla T \right). \tag{2.8}$$

The concentration and temperature fields, which track the position of the fluid–fluid interface and the reacting interface are now restricted to take values between 0 and 1. The dispersive terms in equations (2.7) and (2.8) induce mixing in the vicinity of the fluid–fluid and thermal fronts. In these mixing regions, the density is calculated by linear interpolation between the limiting states according to equation (2.5). The dimensionless numbers B_1 and B_2 are given by,

$$B_1 = \frac{(\rho^*_{inj} - \rho^*_{res})k^* \boldsymbol{g}^* \sin\theta}{\mu^* U^*}, \qquad B_2 = \frac{(\rho^*_{injT} - \rho^*_{inj})k^* \boldsymbol{g}^* \sin\theta}{\mu^* U^*}, \tag{2.9}$$

where ρ^*_{inj} is the density of the injected fluid downstream of the reaction, where it has the same temperature as the reservoir and ρ^*_{injT} is the density of the injected fluid at temperature $T^*_{res} + \Delta T^*$. In the calculations, the inverse Péclet number, D, was chosen to be 5.0×10^{-3} except where otherwise stated. Equations (2.5) and (2.6) were solved in a quadratic domain $(x, y) \in [0, 1] \times [0, 1]$ using a mixed finite-element method (e.g. Brezzi & Fortin 1991) with Dirichlet conditions for the velocity components. A conservative finite-volume method (see Nigam 2003) was applied for the solution of equations (2.7) and (2.8). Inflow conditions for C and T were specified at the source. In all calculations, the source is located at $x = 0.5,\ y = 0.75$, the sink at $x = 0.5,\ y = 0.25$, and their radii are both 0.05. The grid-parameter, defined as $h = \sqrt{2A^e_{max}}$ (where A^e_{max} is the maximum area of the triangular finite elements) was chosen to be $2D$, and the time-step, Δt, was chosen to be $D/2$. The calculations were carried out for t between 0 and $5\,t_{sweep}$, where t_{sweep} is the time required to inject a volume of fluid equivalent to the volume of the reservoir. Displacement patterns in figures 1, 3 and 4 are shown at $t = (\pi/100)t_{sweep}$, $(\pi/20)t_{sweep}$, t_{sweep} and $5t_{sweep}$. The parameters for the different runs are summairzed in table 1.

3. Results

3.1. *Isothermal flows*

In figure 1, we present a series of calculations which illustrate how the flow pattern develops with time in the case where the density of the injected fluid differs from that of the reservoir fluid, but with no thermal reaction. Each case corresponds to a different value of the buoyancy number, B_1. For each case, the four panels (left to right) correspond to the zone of the reservoir occupied by the injected fluid at the four dimensionless times $(\pi/100)t_{sweep}$, $(\pi/20)t_{sweep}$, t_{sweep} and $5t_{sweep}$.

Case A3 (figure 1*c*) corresponds to the simple displacement flow in which there are no gravity effects. This is the reference calculation with which the remaining calculations, which include density contrasts, may be compared. In figure 1(*c*), it is seen that the injected fluid gradually displaces the reservoir fluid, but once the injected fluid begins to break through to the producing well, the rate of displacement

Run	B_1	B_2	λ	D
A1	−1	–	–	5.0×10^{-3}
A2	−0.25	–	–	5.0×10^{-3}
A3	0	–	–	5.0×10^{-3}
A4	0.25	–	–	5.0×10^{-3}
A5	1	–	–	5.0×10^{-3}
B1	−1	–	–	1.0×10^{-2}
B2	−0.25	–	–	1.0×10^{-2}
B3	0	–	–	1.0×10^{-2}
B4	0.25	–	–	1.0×10^{-2}
B5	1	–	–	1.0×10^{-2}
C1	0.25	−1	0.25	5.0×10^{-3}
C2	0.25	−1	0.5	5.0×10^{-3}
C3	0.25	−1	0.75	5.0×10^{-3}
D1	0.25	−0.25	0.25	5.0×10^{-3}
D2	0.25	−0.25	0.5	5.0×10^{-3}
D3	0.25	−0.25	0.75	5.0×10^{-3}
E1	0.25	0	0.25	5.0×10^{-3}
E2	0.25	0	0.5	5.0×10^{-3}
E3	0.25	0	0.75	5.0×10^{-3}
F1	0.25	1	0.25	5.0×10^{-3}
F2	0.25	1	0.5	5.0×10^{-3}
F3	0.25	1	0.75	5.0×10^{-3}
G1	0.25	−1	0.5	1.0×10^{-2}
G2	0.25	−0.25	0.5	1.0×10^{-2}
G3	0.25	0	0.5	1.0×10^{-2}
G4	0.25	1	0.5	1.0×10^{-2}
H1	−0.25	−1	0.25	5.0×10^{-3}
H2	−0.25	−1	0.5	5.0×10^{-3}
H3	−0.25	−1	0.75	5.0×10^{-3}
I1	−0.25	0	0.25	5.0×10^{-3}
I2	−0.25	0	0.5	5.0×10^{-3}
I3	−0.25	0	0.75	5.0×10^{-3}
J1	−0.25	0.25	0.25	5.0×10^{-3}
J2	−0.25	0.25	0.5	5.0×10^{-3}
J3	−0.25	0.25	0.75	5.0×10^{-3}
K1	−0.25	1	0.25	5.0×10^{-3}
K2	−0.25	1	0.5	5.0×10^{-3}
K3	−0.25	1	0.75	5.0×10^{-3}
L1	−0.25	−1	0.5	1.0×10^{-2}
L2	−0.25	0	0.5	1.0×10^{-2}
L3	−0.25	0.25	0.5	1.0×10^{-2}
L4	−0.25	1	0.5	1.0×10^{-2}

TABLE 1. Parameters for computations with buoyancy contrasts.

of reservoir fluid decreases rapidly, so that after five pore volumes have been injected, only 95 % of the fluid has been swept. In cases *a* and *b*, the injected fluid is less dense than the reservoir fluid. In case A1, the buoyancy force dominates the applied pressure gradient associated with the flow, and the injected fluid rises to the top of the reservoir, and then gradually fills the reservoir. This leads to a large fraction of the reservoir volume being flooded with injected water.

Conversely, cases A4 and A5 correspond to the situation in which the injected fluid is denser than the host fluid, in which case the injected fluid forms a narrower plume

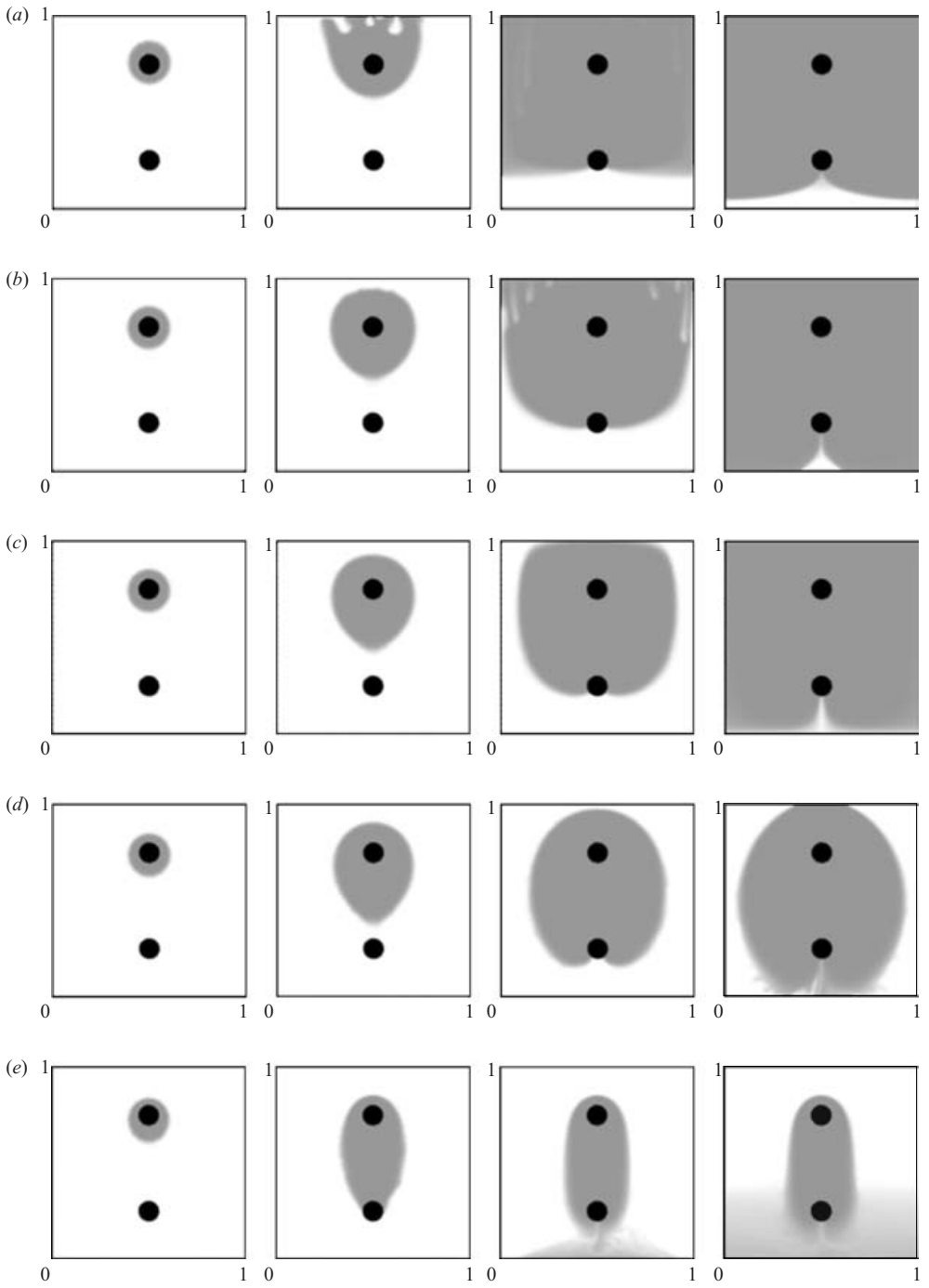

FIGURE 1. Isothermal ($T = 0$) displacement patterns for runs (*a*) A1: $B_1 = -1$, (*b*) A2: $B_1 = -0.25$, (*c*) A3: $B_1 = 0$, (*d*) A4: $B_1 = 0.25$ and (*e*) A5: $B_1 = 1$.

migrating to the sink. In both cases, owing to the density of the fluid, some of the injected fluid runs past the sink, and displaces fluid at the base of the zone.

These reference calculations provide some insight into the underlying control of gravity on the flow pattern. One prediction of the models is the increase in the

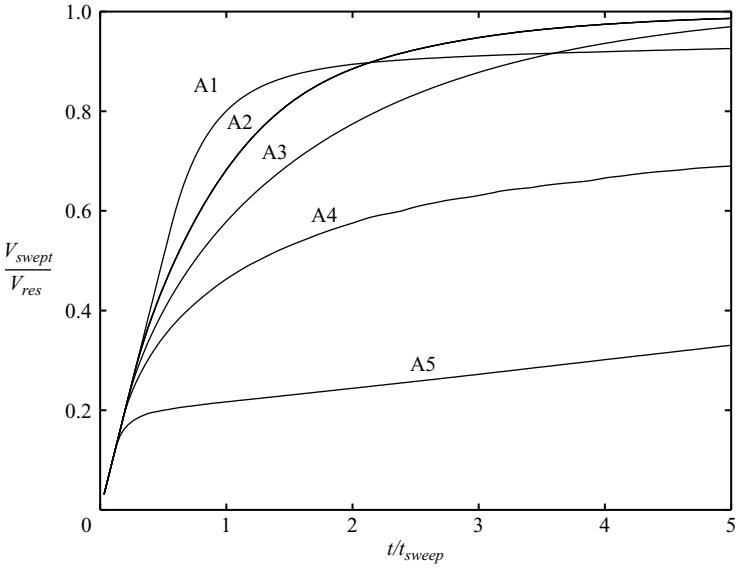

FIGURE 2. Production plots for runs A1, A2, A3, A4 and A5.

area of the domain which is invaded with injected water as a function of the total volume injected (figure 2). For the case of a dense fluid which channels through to the producing well, the area which is invaded by the injected fluid is the smallest. In contrast, for the case of a relatively buoyant injectate, the fraction of the area which is invaded by the injectate initially increases most rapidly as a function of the total volume of fluid injected. This is a result of the ascent of the fluid to the top of the domain, and the subsequent displacement of the reservoir fluid towards the sink. However, once the injected liquid has invaded the zone above the sink, it tends to flow into the sink rather than continuing to displace the fluid below. As a result, the area invaded with injected liquid increases ever more slowly as a function of the volume injected. Eventually, for sufficiently large injected volume, it is surpassed by the area invaded by a fluid of the same density as the host fluid, which is able to displace more of the fluid below the sink.

We now explore how these results change when there is a temperature contrast between the injected and the host fluid which has an attendant density change.

3.2. *The effect of thermal and compositional fronts*

If there is a thermal front which lags the fluid–fluid front owing to the thermal inertia (Fayers 1962), then the range of flow patterns becomes considerably richer. In examining the effect of density changes across such fronts, one key parameter is the magnitude and sign of the dimensionless buoyancy jump across the thermal front, B_2 (equation (2.9)), in comparison to that across the fluid–fluid front, B_1. Figure 3(*a–c*) compares a series of calculations for which the density of the injected liquid, after passing through the thermal front, is greater than that of the reservoir fluid. In figure 3(*a*), the density of the injected fluid, prior to passing through the thermal front, is much less dense than the thermally adjusted fluid, and hence the dark zone nearest the source tends to migrate upwards through the thermally adjusted injected fluid.

Once the fluid at the original injection temperature has invaded the zone at the top of the domain, the thermal front then migrates downwards towards the sink. This

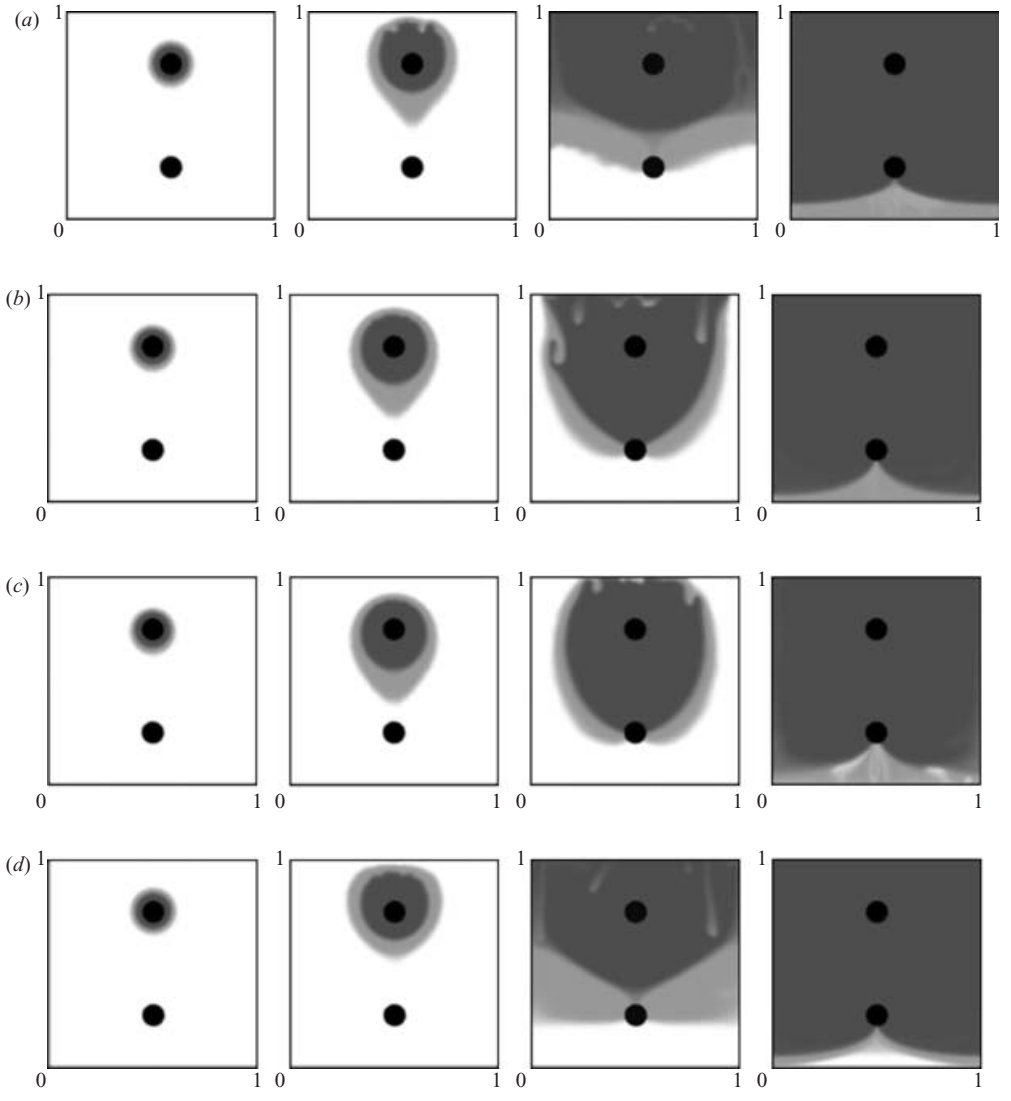

FIGURE 3. Displacement patterns with $\lambda = 0.5$ for runs (*a*) C2: $B_1 = 0.25,\ B_2 = -1$, (*b*) D2: $B_1 = 0.25,\ B_2 = -0.25$, (*c*) E2: $B_1 = 0.25,\ B_2 = 0$ and (*d*) H2: $B_1 = -0.25,\ B_2 = -1$.

displaces the injected water located ahead of the thermal front, which has adjusted to the temperature of the formation. In turn, this displaces the reservoir fluid from the domain. In figure 3(*b*), the fluid which is injected into the domain has the same density as the reservoir fluid. However, the thermal front produces an intermediate zone within which fluid is denser than the reservoir fluid. As a result, the injected fluid ahead of the thermal front tends to flow in a narrow plume towards the sink, but the continuing injected fluid behind the flow front displaces a greater volume of the reservoir fluid, since it is neutrally buoyant, and eventually asymptotes towards a simple source–sink flow with no buoyancy effects. In figure 3(*c*), there is no density change across the thermal front, and so the injected fluid remains dense relative to the reservoir fluid. This figure provides a useful reference for cases C2 and D2 in which the change in density across the thermal front has a major impact on the flow

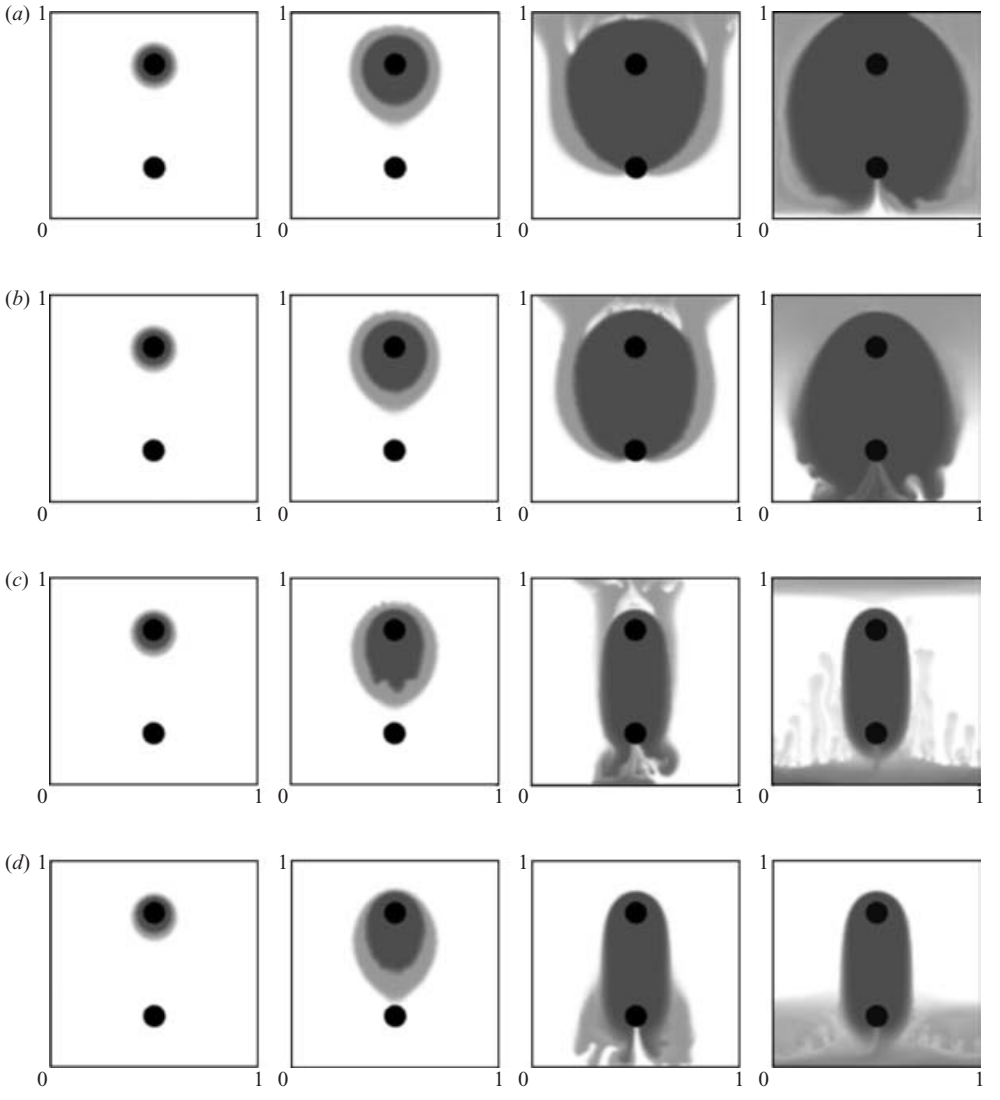

FIGURE 4. Displacement patterns with $\lambda = 0.5$ for runs (*a*) I2: $B_1 = -0.25,\ B_2 = 0$, (*b*) J2: $B_1 = -0.25,\ B_2 = 0.25$, (*c*) K2: $B_1 = -0.25,\ B_2 = 1$ and (*d*) F2: $B_1 = 0.25,\ B_2 = 1$.

pattern and evolution. Figure 3(*d*) corresponds to the case in which the density of the thermally adjusted fluid is smaller than that of the reservoir fluid, yet the density of the injected fluid prior to thermal adjustment is even smaller. In this case, the flow pattern is reminiscent of case C2, especially once the thermal front has advanced through the domain, and it is the density contrast between the original injectate and the reservoir fluid which dominates the flow pattern. In figure 4(*a–c*), a complementary series of calculations are presented to illustrate the flow pattern in the case in which the density of the thermally adjusted fluid is smaller than the density of the reservoir fluid. In case I2 there is no change in density across the thermal front, and the flow pattern is analogous to figure 1(*b*). In case J2, the density of the injected fluid is the same as that of the reservoir fluid, but the injected fluid becomes less dense as it passes through the thermal front. As a result, once the thermal front has advanced to

the sink, the thermally adjusted fluid ahead of this front begins to rise and accumulate at the top of the domain. Meanwhile, the continuing supply of fluid at the original injection temperature flows directly to the sink. In case k2, the input liquid is much denser than the reservoir fluid, but after thermal adjustment, the injected fluid is less dense than the reservoir fluid. As a result, the zone of thermally adjusted fluid tends to ascend to the top of the reservoir, while the continuing original injectate descends in a rather narrow dense plume towards the sink, in an analogous manner to figure 1(*e*). Figure 4 also includes the case in which the injected fluid is denser than the reservoir fluid, but in which the thermally adjusted fluid is even more dense. Initially, the thermally adjusted fluid descends downwards more quickly than the continuing stream of original fluid behind the front. However, once the thermal front reaches the sink, a narrow dense plume of original injectate flows down to the sink, and the thermally adjusted fluid accumulates on the base of the domain.

These calculations have shown that the initial flow pattern depends largely on the density contrast between the injected fluid after thermal adjustment and the reservoir fluid. However, at longer times, when the thermal front reaches the sink, the flow pattern becomes dominated by the density contrast between the injected fluid before thermal adjustment and the reservoir fluid. This evolution of the flow pattern is captured in figure 5 which illustrates how the area of the domain which is invaded by the injected fluid changes with volume injected. In each panel of figure 5, three curves are given corresponding to different rates of propagation of the thermal reaction front compared to the fluid–fluid front.

3.3. *Sensitivity to parameterization of dispersion*

The numerical scheme used to solve these interface displacement problems introduced concentration and temperature fields to define the location of the interface. These concentration fields were then allowed to diffuse across the interface to model the dispersive mixing, which in the present application is relatively small. To test that in our calculations this mixed dispersion zone remains small and has a secondary impact on the quantitative results of the calculations, we have re-calculated some of the cases using a dispersive mixing coefficient which is twice as large. Figure 6 illustrates the ratio of the fraction of liquid swept from the reservoir for the two values of the dispersion coefficient. It is seen that the errors associated with this approach are very small.

4. Discussion and conclusion

In this paper, we have examined the effect of density contrasts between the injected and the reservoir fluid in a two-dimensional source–sink flow in a porous medium, with the sink located below the source. If the injected liquid is denser than the reservoir fluid then the flow tends to become channelled more directly to the sink. As a result, a smaller volume of the reservoir fluid is displaced into the sink prior to the flow of injected liquid into the sink as compared to the case in which the injected fluid has the same density as the reservoir fluid. Conversely, if the injected fluid is less dense than the reservoir fluid, then the injected fluid tends to spread upwards and outwards. As a result, a larger volume of injected liquid must be supplied before it reaches and flows into the sink.

We have then examined the effect of an internal density front within the injected liquid, such as would develop if the injected liquid is of different temperature to the reservoir. In this case, the initial displacement pattern is strongly influenced by

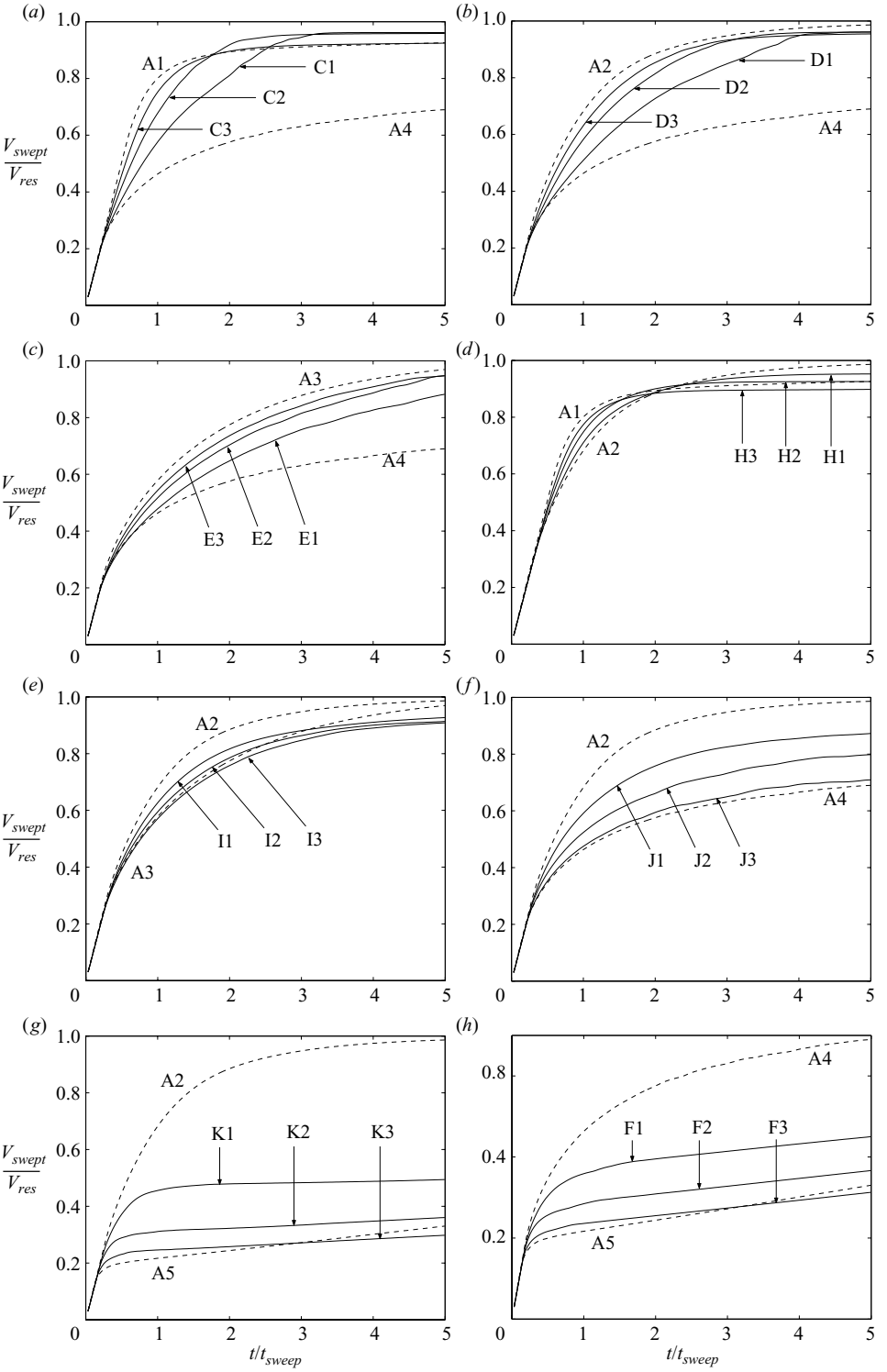

FIGURE 5. Production plots for $\lambda = 0.25$, 0.5 and 0.75 (solid lines). Also shown are the limiting isothermal cases (dashed lines).

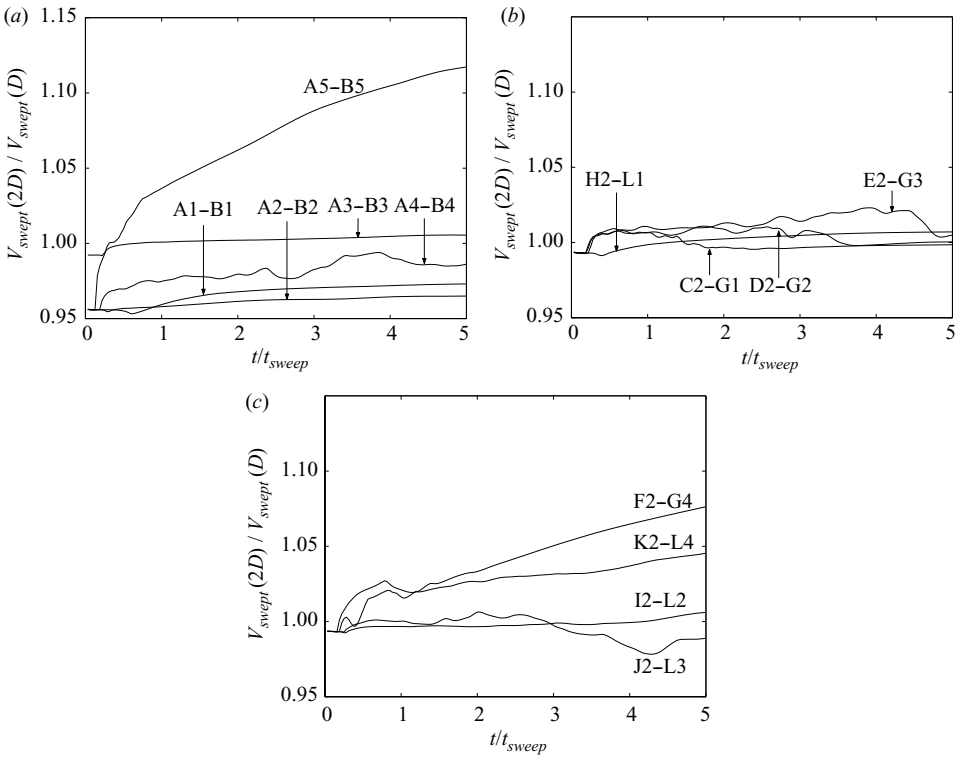

FIGURE 6. The dependence on the dispersion length is shown for (*a*) $B_1 = -1, -0.25, 0, 0.25, 1$ and $B_2 = 0$, (*b*) $B_1 = 0.25$ and $B_2 = -1, -0.25, 0, 1$, and (*c*) $B_1 = -0.25$ and $B_2 = -1, 0, 0.25, 1$.

the density contrast between the thermally adjusted injected fluid and the reservoir fluid. However, once the injected liquid begins to flow into the sink, progressively more of the area filled with injected liquid is not thermally adjusted, and so the displacement pattern evolves towards that associated with the difference between the injected liquid at its original temperature and the reservoir fluid. This can lead to a range of fascinating flow regimes (figures 3 and 4) in which the thermally adjusted injection fluid is buoyant (negatively buoyant) relative to the reservoir fluid, while the raw injected fluid is negatively buoyant (buoyant). In other situations, the thermal adjustment may increase or decrease the buoyancy contrast, leading to channelling or broadening of the flow pattern once the thermal front has moved from the source towards the sink.

These results may have considerable importance in predicting the flow pattern within a natural permeable rock when one fluid is displaced by a second of different density and temperature, as is common in the hydrocarbon and geothermal industries. In both cases, although there is a spectrum of reservoir types, many fields consist of a series of separate thin laterally extensive layers, for which a two-dimensional source–sink flow may represent an appropriate leading-order simplification. The model here strictly describes a miscible displacement flow, and may therefore be most directly applicable to modelling water flooding within geothermal systems (e.g. Woods 1999). However, it also provides useful insight into immiscible displacement flows, in which the front between the two liquids may be described using the Buckley–Leverett theory

(e.g. Bear 1972). That theory predicts that a shock front develops at the front across which there is a finite change in saturation, so that upstream only the reservoir fluid is displaced, while downstream, the injected liquid and some residual fraction of the reservoir fluid both flow. In the limit that the saturation jump is large, then behind this front there may be only a small amount of mobile reservoir fluid, and in this case, our model provides a simplified picture of the flow, assuming the mobility ratio is close to unity.

In both applications, the effect of buoyancy reversal, or at least of a substantial change in the buoyancy, is a realistic scenario. Indeed, typical subsurface reservoirs may have temperatures 50–150 K higher than surface water injected into the system. A change of temperature of this magnitude may lead to a density change of order 10%. In a geothermal system, the water in place in the reservoir is likely to have a different composition to the injected water, leading to density contrasts of 1–10%, comparable to the density change due to the heating of the injected water. Hydrocarbons have a wide range of densities, depending on composition, but a typical value is of order 0.7–0.9 times that of water. In that case, density reversal may be less common, but substantial changes in the magnitude of the buoyancy of injected water are possible.

This work has been supported by the Newton Trust, and the BP Institute, as well as the BP Magnus Team.

Appendix. Viscosity contrasts

Although this work focuses on the role of density contrasts in affecting the structure of a source–sink flow in a porous medium, it is worth noting the impact which a viscosity contrast across this thermal front could also have on the sweep pattern. The calculations in this Appendix are analogous to a series of nonlinear calculations of the interaction between two distinct fronts, across each of which there are different mobility contrasts. As expected from the classical Saffman–Taylor instability (Chouke, van Meurs & van der Poel 1959), the interference of mobility contrasts across either of these fronts can lead to instability if there is an adverse change in the mobility (Gorell & Homsy 1983; Yortsos & Huang 1986) and it is the nonlinear interaction between two such fronts, one of which arises from the temperature contrast, which is of interest here.

Hereinafter, the angle θ in equation (2.1) is set equal to zero (eliminating buoyancy effects) and the viscosity $\mu^*(C,\ T^*)$ is allowed to vary in time and space according to the fluid phase at that point. In mixing regions, the non-dimensionalized viscosity is calculated by linear interpolation between the limiting states,

$$\mu(C,\ T) = \frac{\mu^*_{res}}{\mu^*}\left\{1 + C\left[\left(\frac{\mu^*_{inj}}{\mu^*_{res}} - 1\right) + T\left(\frac{\mu^*_{injT}}{\mu^*_{res}} - \frac{\mu^*_{inj}}{\mu^*_{res}}\right)\right]\right\}, \tag{A 1}$$

where μ^*_{inj} is the viscosity of the injected fluid downstream of the reaction, where it has the same temperature as the reservoir and μ^*_{injT} is the viscosity of the injected fluid at temperature $T^*_{res} + \Delta T^*$. The reference viscosity is chosen to be

$$\mu^* = min\left[\mu^*_{res},\ \mu^*_{inj},\ \mu^*_{injT}\right], \tag{A 2}$$

in order to limit $|\boldsymbol{u}|$ between 0 and the source–sink value, 1. In the calculations, the inverse Péclet number, D, was chosen to be 5.0×10^{-3} except where otherwise stated. The calculations were carried out for t between 0 and $5\,t_{sweep}$, and the displacement

Run	μ^*_{inj}/μ^*_{res}	μ^*_{injT}/μ^*_{res}	λ	D
A	1	–	–	5.0×10^{-3}
B	0.1	–	–	5.0×10^{-3}
C	10	–	–	5.0×10^{-3}
G	1	0.1	0.25	5.0×10^{-3}
H	1	0.1	0.5	5.0×10^{-3}
I	1	0.1	0.75	5.0×10^{-3}
J	0.1	1	0.25	5.0×10^{-3}
K	0.1	1	0.5	5.0×10^{-3}
L	0.1	1	0.75	5.0×10^{-3}
M	1	10	0.25	5.0×10^{-3}
N	1	10	0.5	5.0×10^{-3}
O	1	10	0.75	5.0×10^{-3}
P	10	1	0.25	5.0×10^{-3}
Q	10	1	0.5	5.0×10^{-3}
R	10	1	0.75	5.0×10^{-3}

TABLE 2. Parameters for computations with mobility contrasts.

patterns in figures 7 and 9 are shown at $t = (\pi/100)t_{sweep}$, $(\pi/20)t_{sweep}$, t_{sweep} and $5t_{sweep}$. The parameters for the different runs are summarized in table 2.

We have selected three values of the mobility ratio, to illustrate the effect of an increase and decrease in mobility ratio across the fluid–fluid front. We then extend these calculations by including the thermal front, across which we assume there is a change in mobility of the injected fluid, and we compare these more complex flows with their isothermal counterparts. The aim of these calculations is to gain quantitative insight into the structure and evolution of the flow.

A.1. *Isothermal flows*

In figure 7, we present a series of calculations which illustrate how the flow pattern develops with time in the case where the viscosity of the injected fluid differs from that of the reservoir fluid, but with no thermal reaction. This reference set of calculations is analogous to the results of Chen & Meiburg (1998*a*). Case A (figure 7*a*) corresponds to the simple displacement flow in which there is no mobility ratio. This is the reference calculation for the subsequent calculations which include changes in the mobility ratio. It is seen that the injected fluid gradually displaces the reservoir fluid, but once the injected fluid begins to break through to the producing well, the rate of displacement of reservoir fluid decreases rapidly, so that after five pore volumes have been injected only 95% of the fluid has been swept. When the mobility of the injected fluid is smaller than the reservoir fluid, then the interface tends to be unstable to Saffman–Taylor fingering (figure 7*b*) (cf. Chuoke *et al.* 1959). However, the background pressure field associated with the source–sink flow leads to preferential growth of the fingering towards the sink, and a dominant channel develops which allows the injected fluid to bypass much of the reservoir fluid, and flow directly into the sink. This leads to a much smaller fraction of the fluid being swept (figure 7*b*). In the other limit, in which the injected fluid is less mobile than the reservoir fluid, the interface is very stable, and the injected fluid initially tends to spread radially from the source, while the reservoir fluid of higher mobility follows a more tortuous path to the sink (figure 7*c*). To summarize these results, in figure 8 we illustrate how the fraction of the reservoir which is flooded with injected fluid increases as a function of the total volume of fluid

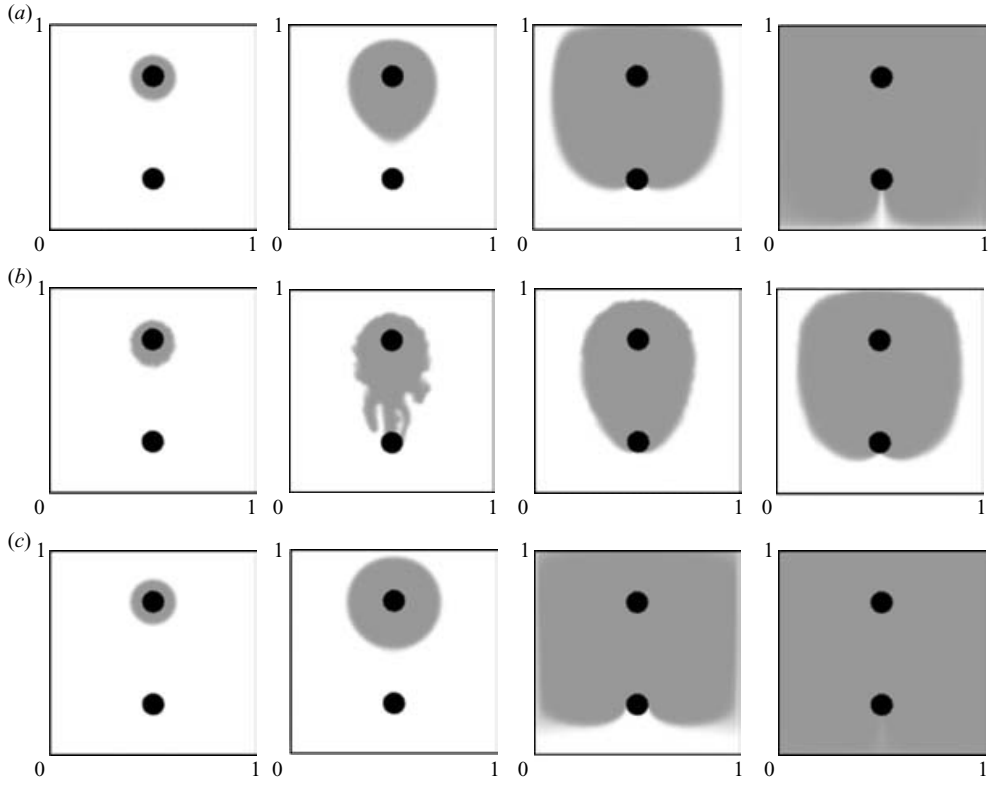

FIGURE 7. Isothermal ($T=0$) displacement patterns for runs (a) A: $\mu^*_{inj}/\mu^*_{res}=1$, ($b$) B: $\mu^*_{inj}/\mu^*_{res}=0.1$ and (c) C: $\mu^*_{inj}/\mu^*_{res}=10$.

injected. In general, the lower the mobility of the injected fluid, the greater the sweep efficiency produced by the injection process.

A.2. *The effect of thermal and compositional fronts*

The change in mobility across a thermal front may be significant, especially if there is a reaction associated with the change in temperature. Indeed, the permeability change may be comparable to the difference in viscosity between the injected fluid and the reservoir fluid, especially when the temperature contrasts are large, and in the hydrocarbon situation, the oil is light and of low viscosity. In the present model, the key parameter which determines the motion of the interface is the mobility ratio, given by the product of the viscosity ratio and the inverse of the permeability ratio. A second variable of importance is the location of the thermal or reaction front relative to the fluid–fluid front, since the advection speed of the thermal front relative to the fluid front varies with the porosity of the rock, and also the ratio of the specific heat of the fluid and the rock (Phillips 1991). This second parameter determines the time scale over which the thermal reaction has a key impact on the flow pattern. We now present two sets of calculations to illustrate the importance of each of these effects. First, we show the evolution of the fluid–fluid front and the thermal front, for four different cases.

In figure 9(a) the injected fluid has a viscosity 0.1 times that of the reservoir fluid, while the fluid which has passed through the thermal front has a viscosity equal to

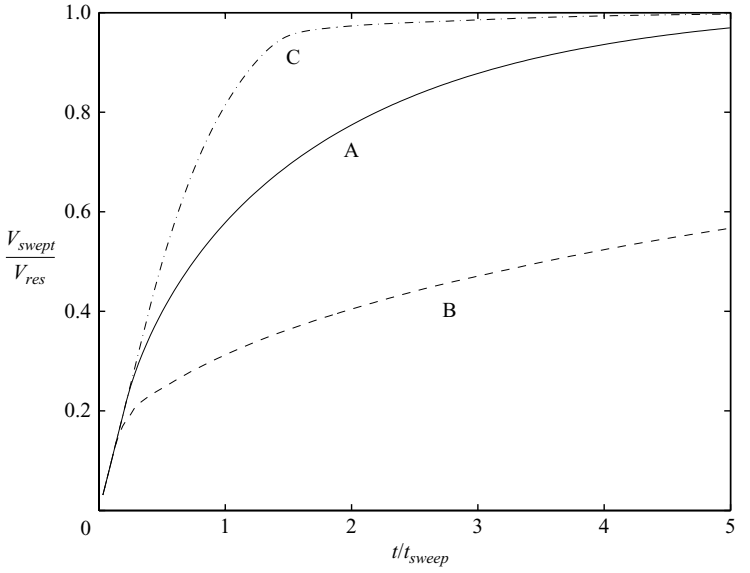

FIGURE 8. Production plots for runs A, B and C.

that of the reservoir fluid. This situation may arise for example across a cooling front. As a result, the thermal front is unstable, and the original fluid behind the thermal front tends to finger through the interface. However, there is no mobility contrast across the interface between the injected and the original reservoir fluid, and this remains stable. The initial displacement pattern of the fluid which is ahead of the thermal front is analogous to the reference case of figure 7(*a*). However, as the thermal front spreads from the source, the influence of the mobility ratio across the thermal front becomes progressively more fingered, and this tends to create a channel which connects the low-viscosity injected fluid directly to the sink, bypassing some of the earlier injected fluid which has propagated through the thermal front and has become more viscous. Subsequently, the propagation of the thermal front is much slower, and the flow pattern and volume of reservoir fluid which is swept to the sink tends to that of case B shown in figure 7(*b*) (see figure 10*a*).

In figure 9*b* the injected fluid upstream of the thermal front has the same mobility as the reservoir fluid, while the injected fluid downstream of the thermal front has a lower viscosity and is therefore unstable as it displaces the reservoir fluid. The interface therefore tends to finger into the reservoir fluid, and a channel begins to develop towards the sink, with much of the reservoir fluid being bypassed as in case B (see figure 10*b*). However, as the thermal front grows out from the source, the higher viscosity of the fluid behind the thermal front begins to influence the overall flow pattern more dominantly. Eventually, the thermal front no longer influences the leading-order structure of the flow, which evolves back towards the flow pattern of figure 7(*a*), in which there is no mobility ratio across the fluid–fluid front. As a result, the volume of the fluid swept from the reservoir increases towards the reference curve, case A (see figure 10*b*).

In figure 9(*c*), the injected fluid has a viscosity 10 times larger than that of the reservoir fluid, but as it passes through the thermal front, the fluid viscosity decreases to that of the reservoir fluid. This regime might correspond to a cooling front. Since the injected fluid ahead of the thermal front has similar viscosity to the reservoir fluid,

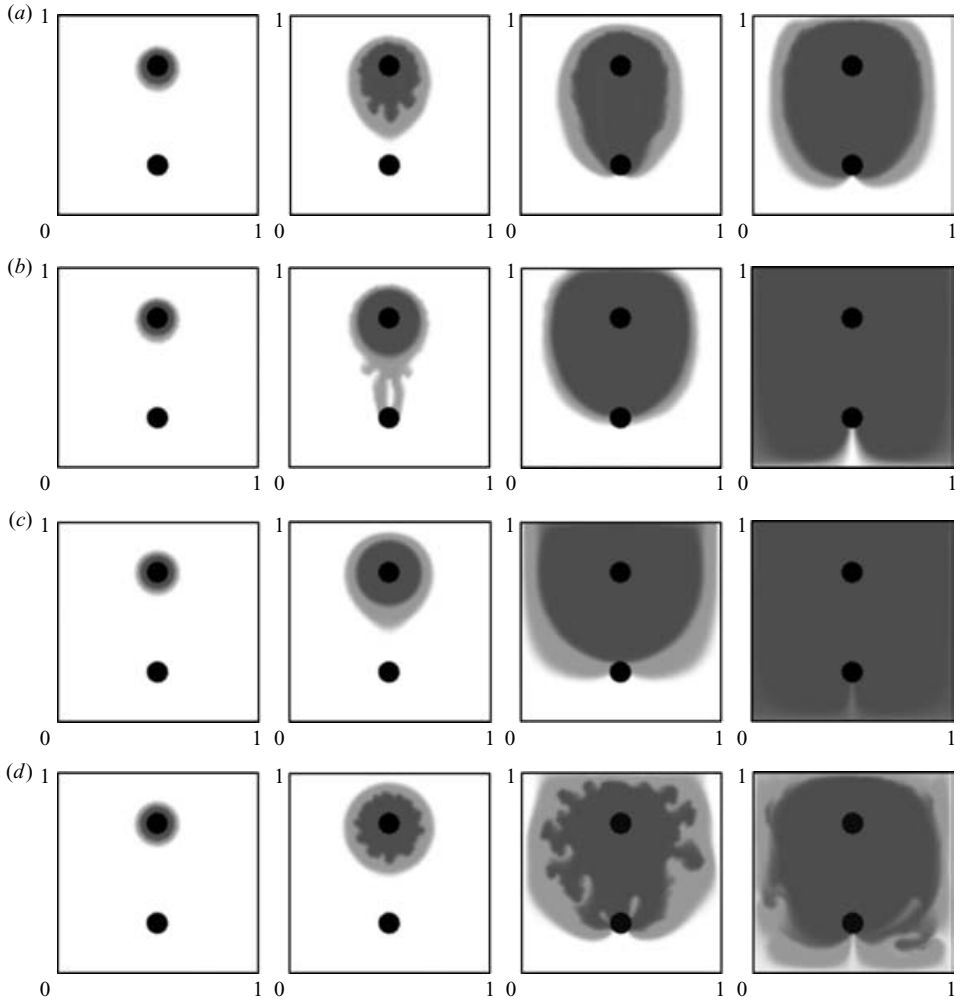

FIGURE 9. Displacement patterns with $\lambda = 0.5$ for runs (*a*) H: $\mu^*_{inj}/\mu^*_{res} = 1$, $\mu^*_{injT}/\mu^*_{res} = 0.1$, (*b*) K: $\mu^*_{inj}/\mu^*_{res} = 0.1$, $\mu^*_{injT}/\mu^*_{res} = 1$, (*c*) N: $\mu^*_{inj}/\mu^*_{res} = 1$, $\mu^*_{injT}/\mu^*_{res} = 10$ and (*d*) Q: $\mu^*_{inj}/\mu^*_{res} = 10$, $\mu^*_{injT}/\mu^*_{res} = 1$.

the flow initially resembles that of case A. However, as the thermal front grows, the much lower mobility of this fluid leads to a more axisymmetric sweep pattern away from the source, and the continuing flow adjusts to a regime analogous to that of case C. As a result, the volume of reservoir fluid which is swept to the sink increases rapidly as the thermal front sweeps through the domain (figure 10*c*).

In contrast to this, in figure 9(*d*), the injected fluid has a viscosity comparable to that of the reservoir fluid, but as the injected fluid passes through the thermal front, it becomes 10 times more viscous. As a result, the initial sweep pattern is dominated by the low-viscosity fluid ahead of the thermal front, and the flow is fairly symmetrical about the source. However, the fluid behind the reaction front begins to finger into the thermal front, and eventually breaks through to the sink, bypassing some of the injected fluid which is now downstream of the thermal front and hence much more viscous. As a result, the injected fluid ahead of the thermal front is swept to the

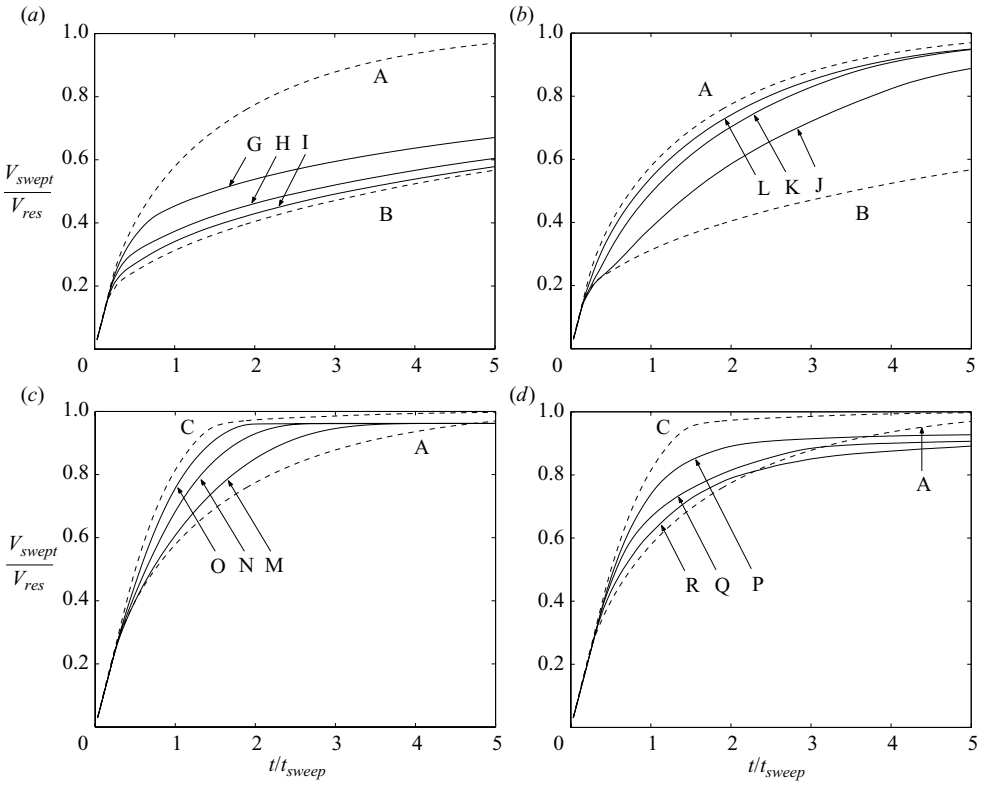

FIGURE 10. Production plots for $\lambda = 0.25$, 0.5 and 0.75 (solid lines). Also shown are the limiting isothermal cases (dashed lines).

boundaries of the system, and the continuing more mobile injected fluid flows directly into the sink, largely without passing through the thermal front, so the sweep pattern adjusts to that of case A (see figure 10*d*).

REFERENCES

BEAR, J. 1972 *Dynamics of Fluids in Porous Media*. Dover.

BREZZI, F. & FORTIN, M. 1991 *Mixed and Hybrid Finite Element Methods*. Springer.

CHEN, C. Y. & MEIBURG, E. 1998*a* Miscible porous media displacements in the quarter five-spot configuration. Part 1. The homogeneous case. *J. Fluid Mech.* **371**, 233–268.

CHEN, C. Y. & MEIBURG, E. 1998*b* Miscible porous media displacements in the quarter five-spot configuration. Part 2. Effect of heterogeneities. *J. Fluid Mech.* **371**, 269–299.

CHEN, C. Y. & MEIBURG, E. 1999 Miscible porous media displacements in the quarter five-spot configuration. Part 3. Non-monotonic viscosity profiles. *J. Fluid Mech.* **388**, 171–195.

CHUOKE, R. L., VAN MEURS, P. & VAN DER POEL, C. 1959 The instability of slow, immiscible, viscous liquid–liquid displacements in permeable media. *Trans. Inst. Mining Metall. Engng* **216**, 188–194.

ELDER, J. W. 1997 *Geothermal Systems*. Academic.

FAYERS, F. J. 1962 Some theoretical results concerning the displacement of a viscous oil by a hot fluid in a porous medium. *J. Fluid Mech.* **13**, 65–76.

GORELL, S. & HOMSY, G. 1983 A theory of optimal policy of oil recovry by secondary displacement processes. *J. Fluid Mech.* **43**, 79–98.

KARAKAS, M., SANEIE, S. & YORTSOS, Y. C. 1986 Displacement of a viscous oil by the combined injection of hot water and a chemical additive. *SPE Res. Engng* 391–402.

Lake, L. W. 1996 Enhanced oil recovery. Prentice Hall.

Loggia, D., Salin, D. & Yortsos, Y. C. 1999 The effect of mobility gradients on viscous instabilities in miscible flows in a porous media. *Phys. Fluids* **10**, 747.

Menand, T., Raw, A. & Woods, A. W. 2002 Thermal inertia and reversing buoyancy in flow in porous media. *Geophys. Res. Lett*. **30**, 1291, doi:10.1025/2002GL016294.

Nigam, M. S. 2003 Numerical simulation of buoyant mixture flows. *Intl J. Multiphase Flow* **29**, 983–1015.

Phillips, O. M. 1991 Flow and reactions in permeable rocks. Cambridge University Press.

Woods, A. W. 1999 Liquid and vapor flow in superheated rock. *Annu. Rev. Fluid Mech.* **31**, 171–199.

Yortsos, Y. C. & Huang, A. B. 1986 Linear stability analysis of immiscible displacement Part 1 – Simple basic flow profiles. *SPE Res. Engng* 378–390 (SPE 12692).